

## **Sustainability of Inorganic Matrix–Grid Composites for Strengthening of Masonry Structures**

**A. Bilotta<sup>1</sup>, F. Ceroni<sup>2</sup>, I. Iovinella<sup>1</sup>, A. Balsamo<sup>1</sup>, E. Nigro<sup>1</sup> and M. Pecce<sup>2</sup>**

<sup>1</sup>**Department of Structures for Engineering and Architecture  
University of Naples Federico II, Italy**

<sup>2</sup>**Department of Engineering, University of Sannio, Italy**

### **Abstract**

Fibre reinforced grout (FRG) composites can provide a strong contribution to the strengthening and preservation of existing masonry building against earthquakes because they exploit good adhesion to masonry structures. The bond behaviour of FRG externally bonded to a masonry substrate is different from that of FRP composites applied by means of epoxy-resin; for some types of fibres embedded in grout layers the debonding can occur inside the composite at the fibre-matrix interface, whereas with FRP the debonding is generally at the composite-masonry interface.

This paper examines the results of experimental bond tests on tuff elements externally strengthened with FRG composites with the aim of studying their bond behaviour. The FRG composite investigated in this study is comprised of a glass fibre net and a non-cementitious matrix applied on both single tuff blocks and prisms made of three tuff blocks connected by mortar joints.

**Keywords:** fibre reinforced grout, strengthening, masonry, bond, experimental tests.

## **1 Introduction**

The use of Fibre Reinforced Grout (FRG) materials for strengthening existing structures is becoming more and more interesting for the scientific community especially for application on masonry elements, due to some advantages compared with the traditional use of epoxy bonded Fiber Reinforced Polymer (FRP) materials. Several experimental studies ([1], [2], [3], [4]) showed that the effectiveness of FRP materials is strongly affected by debonding at the masonry-reinforcement interface. The use of ‘grid’ shaped reinforcements, thanks to their diffuse application, is expected more suitable for masonry elements like walls behaving as ‘bi-dimensional’ elements. Moreover, the grid shape, thanks to a more diffuse distribution of stresses, could be less sensitive to debonding phenomena than FRP

externally bonded strips. However, since in FRG systems the grid is often embedded in a thick grout layer, the behaviour of such composite materials depends sensibly on the grout properties and on its tensile behaviour. Differently from epoxy resins, indeed, the grout is sensible to cracking phenomena and, thus, the bond transfer along the interfaces can be influenced by cracking pattern in the grout layer.

It is worth to note that a wide variability of product are becoming available in the market both in terms of grid and grout for applications on concrete and masonry elements, i.e. for reducing the sensibility of grout to cracking, short fibers can be also added in the mix.

Tension behaviour of the composite system made of grid and grout is, thus, the first aspect that has to be investigated. Experimental studies [5], [6] evidenced that a tri-linear behaviour can be identified:

1. A Linear branch corresponding to an uncracked condition of the grout: in this phase both fiber net and grout collaborate to carry the applied stress and, thus, the stiffness of the experimental law takes into account the contribute of both of them; in particular, the contribute of the grout in this phase is predominant due to its higher thickness.
2. A transition phase where the grout starts cracking and that can be identified by a lower stiffness of the constitutive law compared with the previous branch.
3. A third branch corresponding to a diffuse cracking status in the grout; depending on the grade of cracking, the tensile behaviour of the composite tends to that of the fibers. In this stage, if the grout is completely cracked and the fibers are the only element carrying the applied load, the stiffness of such branch is representative of the stiffness of the only fibers.

The presence of the grout makes, thus, more uncertain the assessment of the mechanical properties of the composite system since the cross section is not uniform along the coupon and is not possible to foresee the number and the position of the cracks; this latter aspect make also more difficult the interpretation of measures of strain gauges.

In [7] the effect of different types of grout and different water/grout ratios on the tension behaviour of the composite system was experimentally investigated. It was observed that the bond between fibers and grout strictly depends on the capacity of grout in permeating the spaces between the rovings of the grid. An improvement of the tensile behaviour was achieved by adding short fibers or polymers in the mortar mix.

Bond tests on masonry supports were also carried out by several researchers ([8], [9], [10], [11]) according to single and double shear set-ups and on both single masonry units and prism made of more bricks. The most common masonry support investigated is made of clay bricks. In [8] it was observed that the values of strain measured by strain gauges are sensible affected by the development and the position of the cracks in the mortar and, thus, are not comparable with the theoretical ones in the loaded section.

Experimental bond tests have also evidenced that when the bonded length increases the tensile failure of the fibers occurs instead of debonding and that the minimum bonded length is probably lower than the values usually estimated for epoxy bonded FRP materials. This can be due to the 'grid' configuration with the

presence of fibers also in the direction orthogonal to the applied load; however, it is worth to note that such a geometrical configuration makes the FRG materials more sensitive to the application procedure, since if the fibers are not well aligned, a not homogeneous distribution of stresses can occur. To avoid this, the pre-curing treatment of the fibers can be useful for facilitating the application procedure.

Experimental tests on masonry panels strengthened with FRG materials on both sides have been carried out by ([13], [14]). In particular, in [13] grid made of carbon fibers embedded in a cementitious matrix have been used for strengthening tuff masonry panels and the tests have evidenced a failure of the strengthened panels due to debonding of the reinforcement from the support. In [14] adobe masonry panels were strengthened with polymeric geo-nets (polyester or polypropylene grids) embedded in adobe-based mortar. The strengthening system allowed a load increase of only 20-30% compared to the un-strengthened wall, but an ultimate displacement increment of about +23% and +83%, respectively, for the polyester or polypropylene geo-nets.

## 2 Experimental Programme

The experimental program is made of bond tests on tuff masonry elements superficially bonded with a glass grid applied by means of a grout. Specimens were tested according to a single-shear pull-push set-up at the Laboratory of Materials and Structures of the University of Sannio.

### 2.1 Tuff and mortar properties

Two types of yellow tuff have been used for preparing the specimens, labelled as NA and BN. Yellow tuff is commonly found in many areas of Southern Italy for building masonry structures. Uniaxial compression tests were carried out on cubes with nominal side of 100 mm, while flexural tests carried out on prisms with dimensions 40 mm x 40 mm x 160 mm (span length 100 mm). The average values of compressive strength,  $f_{cm}$ , and flexural strength,  $f_{ctm}$ , are listed in Table 1 with the correspondent values of Coefficient of Variation (CoV); n is the number of tested samples. Experimental results show a relevant scatter of tensile strength for tuff type NA.

Tuff	n	$f_{cm}$	CoV	n	$f_{ctm}$	CoV
		[MPa]	[%]		[MPa]	[%]
NA	6	5.37	8	4	1.5	38
BN	4	5.81	14	3	1.3	6

Table 1: Mechanical properties of tuff blocks

The higher value of CoV for the tensile strength of tuff type NA evidences that it is more heterogeneous, nevertheless the higher strength (+15%), than the tuff type BN because of some physical properties of the material (porosity, presence of inclusions, etc...) that can locally influence the mechanical properties. The tensile strength is about 25% of the compressive one for both types of tuff.

Specimens can be divided in two groups, each of them constituted of six samples. For the first group, the support was made of single tuff blocks with dimensions  $L = 360$  mm for tuff type BN and 390 for tuff type NA,  $b = 250$  mm and  $h = 110$  mm. The second group consisted of masonry prisms made of three blocks of tuff type NA and two mortar joints. The first unit had dimensions of  $150 \times 250 \times 110$  mm, while the following two had dimensions of  $120 \times 250 \times 110$  mm. The mortar joints' thickness was 10 mm. The total dimensions of the masonry prism were, thus,  $L = 410$  mm,  $b = 250$  mm and  $h = 110$  mm.

Mortar joints were made with two types of pre-mixed natural hydraulic lime and pozzolana-based mortar, with addition of natural sand and without cement. For the mortar type '*Mape-Antique MC*', named in the following M1, three flexural tests were carried out on mortar prisms with dimensions  $40 \text{ mm} \times 40 \text{ mm} \times 160 \text{ mm}$  (span length 100 mm) after 28 days of curing. On the halves parts of the tested specimens compressive tests were also carried out. For the mortar type '*Mape-Antique Allettamento*', named in the following M2, only compressive tests on cubes side 100 mm were realized. The average values of compressive strength,  $f_{cm}$ , and flexural strength,  $f_{ctm}$ , are listed in Table 2 with the correspondent values of *CoV*;  $n$  is the number of tested samples. For the mortar M1 the tensile strength is about 25% of the compressive one.

Mortar	n	$f_{cm}$	CoV	n	$f_{ctm}$	CoV
		[MPa]	[%]		[MPa]	[%]
Mape-Antique MC – M1	6	11.5	9	3	2.8	14
Mape-Antique Allettamento – M2	3	9.4	11	-	-	-
Planitop HDM Restauro	6	17.9	4	3	5.1	20

Table 2: Mechanical properties of mortar and grout

## 2.2 Specimen for peeling and bond tests

The FRP reinforcement is made of a bi-directional pre-cured glass fibers balanced net with rovings spaced of 25 mm in both direction (see Figure 1). The equivalent area is  $35.27 \text{ mm}^2/\text{m}$ , the nominal values of Young's modulus, tensile strength and ultimate strain furnished by producer are 72 GPa, 45 kN/m, and 1.8%, respectively. The FRP grid was bonded over a length  $L_b = 330$  mm and  $L_b = 350$  mm, respectively in case of single blocks or masonry prisms. In the first case, the reinforcement was bonded over a surface without discontinuities (Figure 2a), while in the latter it was applied in order to intersect both mortar joints (Figure 2b). For both groups of specimens the reinforcement was not bonded in the first 30 mm of the tuff support and the width was  $b_f = 120$  mm, corresponding to a ratio  $b_f/b = 0.48$ , and to have 5 rovings in the cross section. The total area of the grid cross section is  $4.30 \text{ mm}^2$ . Before the application of the reinforcement, the surface of specimens was cleaned from dust residuals by compressed air.

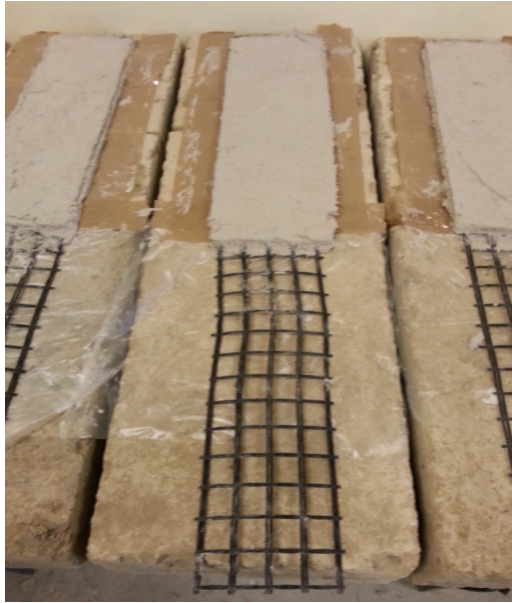


Figure 1: Glass net applied on tuff blocks

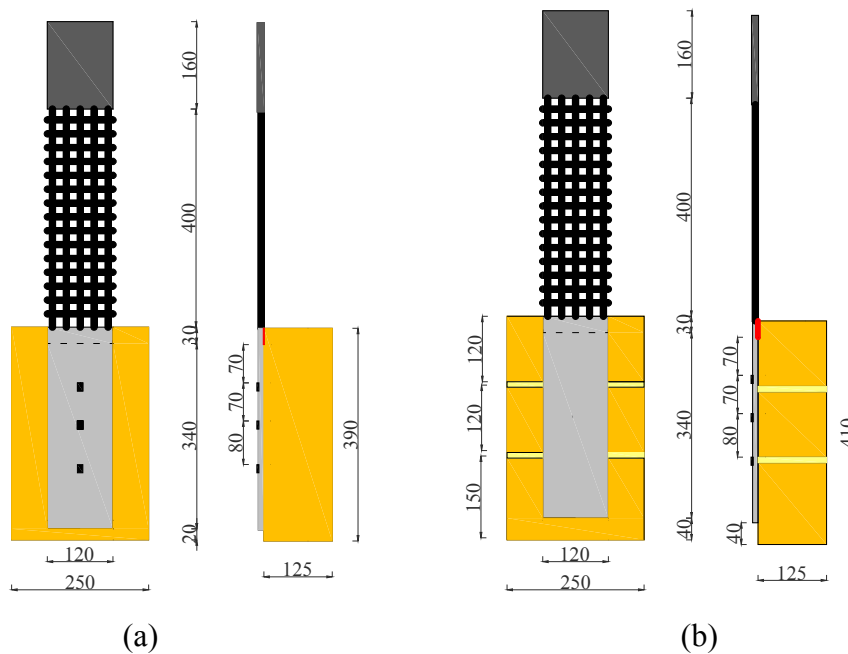


Figure 2: Masonry specimens and position of strain gauges: a) single block; b) prism (dimensions in mm)

The FRP grid was applied by means of a bi-component premixed pozzolana-based mortar made also of hydraulic natural lime, sand, special additives, polymers, and short glass fibers spread in the matrix (*Planitop HDM Restauro*). Thickness of mortar for applying the grid was 10 mm; in particular, a first layer of mortar of 5 mm was applied on the tuff surface, then the grid was positioned and pressed and a second layer of 5 mm of mortar was placed above. Three flexural tests were carried out on mortar prisms with dimensions 40 mm x 40 mm x 160 mm (span length 100

mm) after 28 days of curing. On the halves parts of the tested specimens compressive tests were also carried out. The average values of compressive strength,  $f_{cm}$ , and flexural strength,  $f_{ctm}$ , are listed in Table 2 with the correspondent values of  $CoV$ . The tensile strength is about 28% of the compressive one. The nominal Young's modulus furnished by the producer,  $E_{grid}$ , is 8000 MPa, while the minimum compressive strength is 15 MPa, that has been overcome by the average experimental value.

Specimens made of single tuff blocks (SB) were realized using both types of tuff (BN and NA), while specimens made of masonry prisms (MP) were realized using only tuff type NA, but with two types of mortar for the joints. All specimens were instrumented with 3 strain gauges glued over the central roving of the FRP net (see Fig. 2).

The specimens were tested in a horizontal testing machine that allowed to effectively constrain the blocks and apply the tensile load to the FRP reinforcement, minimizing the difficulties in the alignment of the specimens (see Figure 3). A single-shear pull-push set-up was realized since the masonry specimen was constrained on the loaded side by means of a reaction transversal steel element (height 40 mm) placed onto the front face of the block. In addition, two steel plates, parallel to the FRP strip, were placed on the top surface of the specimen for its whole length and were clamped to the stiff base of the testing apparatus. The unloaded end of the specimen was also blocked by a steel tie that does not constraint the unloaded end of the FRP reinforcement.

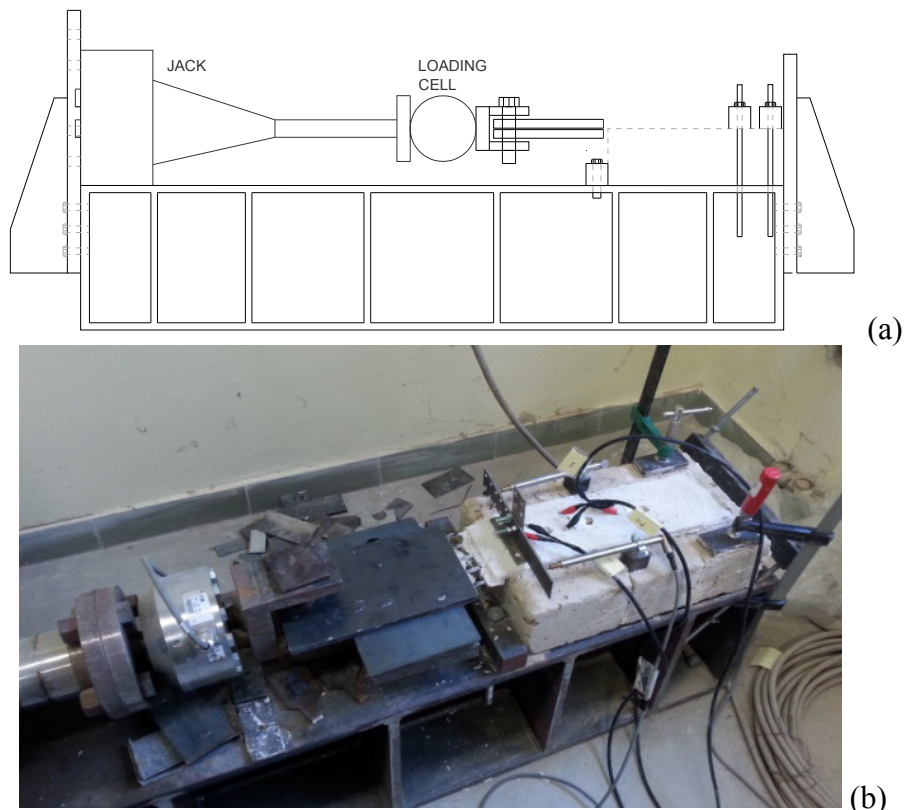


Figure 3: Pull-push test setup: a) scheme; b) photo top view.

### 3 Results

#### 3.1 Tensile tests

Three coupons have been prepared according to the same lay-out and materials used for strengthening the tuff specimens: 1 layer of glass net embedded in a 10 mm thick mortar layer for a total width of 120 mm, i.e. 5 rovings in the cross section, analogously to the specimens prepared for the bond tests (see Figure 4a).

Specimens were instrumented by both three strain gauges (applied on the central roving of glass fibers along one side of the specimen) and two LVDTs (one for each side and a gage measure of 120 mm). As reported in [5] and [6], the coupons for tensile tests are provided at the end of multidirectional FRP sheet epoxy glued for improving the gripping in the testing machine. Such a gripping method has given good results since it allows the application of the tensile load until failure without slipping between the coupon and the grips of the tensile machine. Other types of anchoring lead sometimes to uncorrected failure modes or do not allow to exploiting the maximum strength of the composite system ([5], [6]).

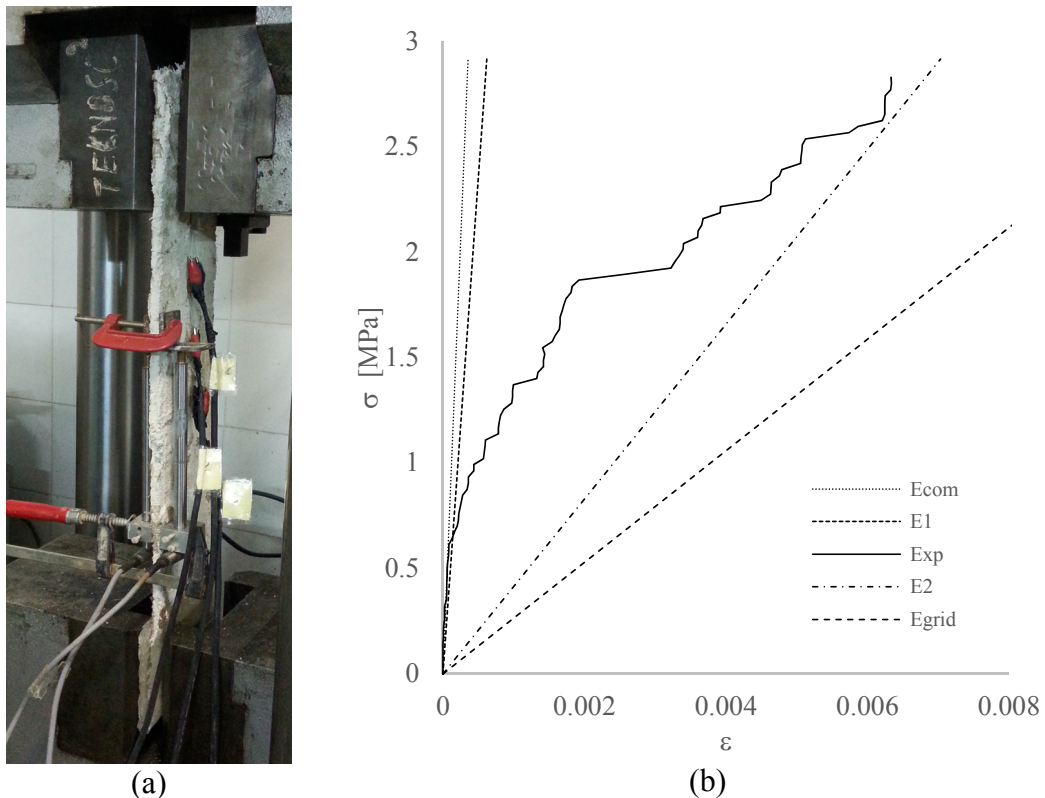


Figure 4: a) Coupon for tensile test; b) Experimental stress-strain relation

The experimental tests demonstrated in all cases the tensile failure of the fibers. Figure 4b shows a typical experimental load-strain relation referring to the measures of strain gauges. Differently from the ‘trilinear’ behaviour evidenced in tensile test by other researchers [5], Figure 4b shows that the transition zone is characterized by

a low variation of slope that could be due to the presence of short glass fibers in the grout and able to give a diffuse tension stiffening effect. Thus, two values of stiffness have been experimentally estimated and reported in Table 3, named  $E_1$  and  $E_2$ . These values were obtained by using the measures of strain gauges. The total area of the cross section was used (10mm x 120mm) in the calculations. In Figure 4b the lines corresponding to the average values of  $E_1$  and  $E_2$  (see Table 3) and the lines corresponding to the nominal stiffness of the only glass grid ( $E_{grid}$ ) and of the composite system ( $E_{com}$ , taking into account both grout and grid contributes) are also graphed.

Note that, after the transition zone, the experimental stiffness does not correspond to the stiffness of the only fibers of the grid ( $E_{grid}$ ), but it is higher. This would mean a residual participation of the grout to carrying the tensile load also after cracking due to the bridging effect of the short fibers added in the mix.

It is worth to note that the difficulty into interpreting the measures of strain gauges, which are affected by the position of the cracks in the grout, highlights the needing of using further measuring systems such as the digital image correlation.

	$E_1$	$E_2$
	[MPa]	[MPa]
PT_1	5322	416
PT_2	4525	406
PT_3	4209	422
Average	4685	415

Table 3: Experimental result of tensile tests

### 3.2 Pull-off tests

Peeling tests were carried out on the surface of tuff block strengthened with the same glass net and grout used for the bond tests. Tests were performed by means of a specific portable testing machine (see Figure 5a) aimed to check the quality of adhesion between different materials by means of a local pull-out tensile test. The testing area is, indeed, limited to a square with side 50 mm where a steel prism is glued in advance by means of an epoxy bi-component resin (MapeWrap 12) having a tensile strength higher than the grout. After a curing time of at least 3 days, the testing area was delimited by cuts in order to avoid whatever contribute of the glass grid (Figure 5b); then the steel prism was screwed to the testing machine in order to apply the tensile load. Tensile load is applied by a handlebars and is visualized on a digital display; load is increased until detachment of the steel prism occurs.

The results are listed in Table 4 in terms of average values of the experimental peeling tensile stress for both types of tuff (NA and BN). Such a tensile stress is calculated by dividing the measured tensile force to the square area 50 mm x 50 mm. Failure occurred in all cases within the tuff with a detachment of a thickness of about 1 mm. In Figure 5c, an example of failure mode is shown. Such a failure mode

highlights that the gluing procedure was correct and the bond is good, since the failure occurred in the weakest element, i.e. the tuff.

Different values of tensile stress were measured for the two types of tuff, nevertheless the tensile strength of the two tuff were comparable (see Table 1); in particular, it can be observed that for the tuff type NA, that was characterized by an higher scatter of experimental values of tensile strength (see Table 1), the lowest value of the tensile peeling stress was achieved with a higher CoV too. In addition, it is worth to note that tuff type NA appeared more heterogeneous than type BN with a more irregular surface texture. Moreover, for tuff type NA the peeling stress was about 17% of the experimental average tensile strength, while for the tuff type BN was about 42% (see Table 1). These results could mean that the peeling strength is related not only to the tensile strength of the support, but primarily to the surface properties of the support in the first millimetres above the bonded reinforcement.

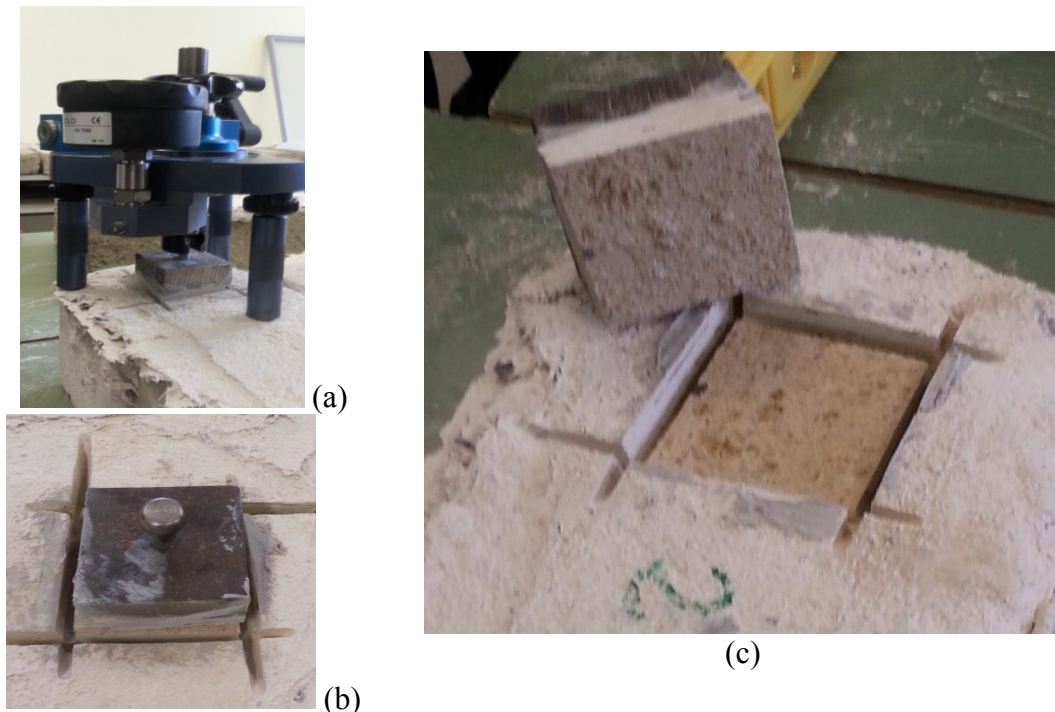


Figure 5: Peeling bond test: a) testing machine; b) application of steel plate; c) failure in the tuff

<b>Tuff</b>	<b>n</b>	<b><math>\sigma_p</math> [MPa]</b>	<b>CoV [%]</b>
NA	6	0.26	55
BN	4	0.54	17

Table 4: Results of peeling bond test

### 3.3 Bond tests

Table 5 lists the main results of bond tests: maximum tensile load for each specimen,  $F_{max}$ , average value of maximum load for equal specimen,  $F_{max,av}$ , and

corresponding  $CoV$ , maximum strain in the unbounded fibres,  $\epsilon_{max}$ , calculated as ratio of  $F_{max}$  to the nominal area (five rovings) and Young's modulus of the grid ( $E_{grid}$ ), the efficiency factor,  $\eta$ , defined as ratio of  $\epsilon_{max}$  to the nominal maximum tensile strain of the glass fibers (1.8%), the maximum experimental strain,  $\epsilon_{max,exp}$ , measured by the first strain gauges applied on a central roving in the bonded length of the reinforcement (see Figure 2).

Specimen ID	Tuff	Mortar	Type of specimen	$F_{max}$ [N]	$F_{max,av}$ [kN]	$\epsilon_{max}$ [%]	$\eta$	$\epsilon_{max,exp}$ [%]
SB_BN_1	BN	-	block	3564	3399 (18%)	1.15	0.78	0.03
SB_BN_2	BN	-	block	2710		0.88	0.59	0.01
SB_BN_3	BN	-	block	3922		1.27	0.86	0.11
SB_NA_1	NA	-	block	3795	3759 (1%)	1.23	0.83	0.27
SB_NA_2	NA	-	block	1795*		-	-	-
SB_NA_2	NA	-	block	3722		1.20	0.82	0.02
MP_NA_M1_1	NA	M1	prism	2767	3179 (29%)	0.89	0.61	0.04
MP_NA_M1_2	NA	M1	prism	4231		1.37	0.93	0.63
MP_NA_M1_3	NA	M1	prism	2538		0.82	0.56	0.37
MP_NA_M2_1	NA	M2	prism	3530	3128 (17%)	1.14	0.77	0.12
MP_NA_M2_2	NA	M2	prism	3323		1.07	0.73	0.65
MP_NA_M2_3	NA	M2	prism	2532		0.82	0.56	0.56

\* grid damaged before testing, not considered in the average value

Table 5: Summary of experimental results of bond tests

The experimental results evidenced that in all tests the tensile failure of the glass fiber of the grid occurred, independently on the type of tuff and on the presence of mortar joints. Specimen SB\_NA\_2 attained a very low failure load due to some damages in the grid before testing; such a result was not considered in the average value. By contrast, the other two specimens of type SB\_NA attained very similar loads ( $CoV=1\%$ ,  $\eta = 0.82$ ).

The experimental values of tensile strain and stress in the grid were lower than the nominal ones given by the producer, i.e. the efficiency factor  $\eta$  ranges between 0.56 and 0.93. These results mean that, nevertheless the same failure mode, the experimental results were quite scattered ( $CoV$  ranges in 17-29%) with exception of the abovementioned series SB\_NA. Such a dispersion of experimental results could be due to the 'grid' configuration of the reinforcement since a non-homogenous distribution of tensile stresses occurs in the rovings of the cross section. In most tests, indeed, the tensile failure of the reinforcement started in the outermost rovings; this led to a loss of symmetry in applying the load respect to the undamaged fibers. Since the failure was not due to debonding, the adhesion of the reinforcement to the support can be considered good, as it was evidenced also by the results of peeling tests, and the bond strength of the FRG-tuff interface was able to allow the tensile failure of the rovings.

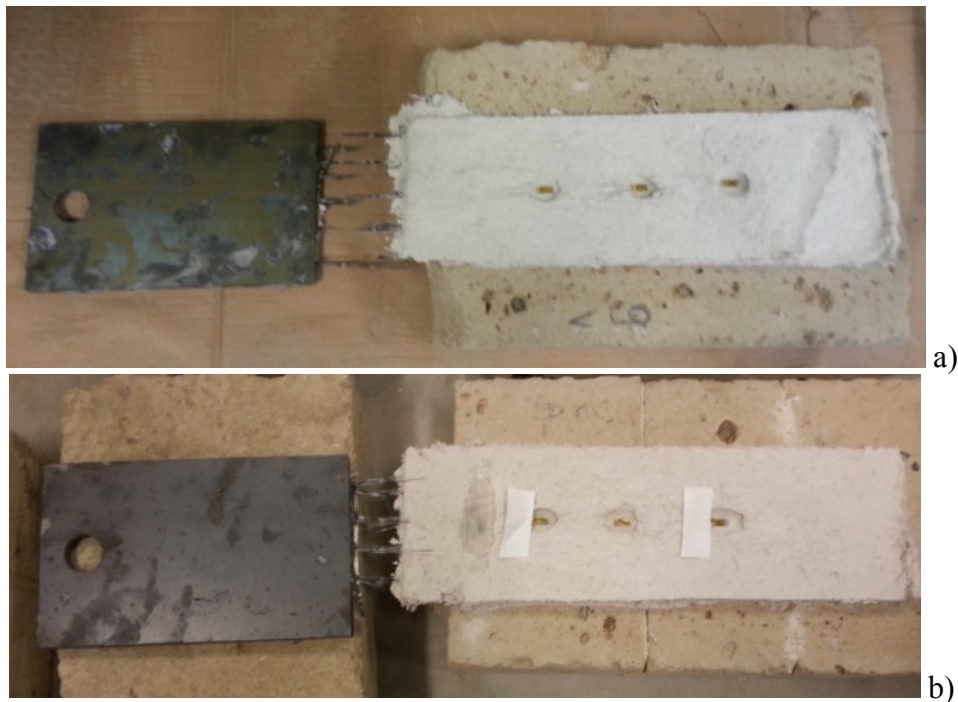


Figure 6: Failure mode of tuff specimens strengthened with glass grid: a) single tuff block; b) tuff masonry prism.

The differences in the behaviour of specimens made of the two different tuff types and of the specimens made by single blocks or prisms were not relevant. In particular, with refer to the average values of load, the specimens made of tuff type NA attained failure load about 10% higher than the specimens made of tuff type BN, but this difference can be considered within the experimental scatter. Moreover, with refer to the specimens with mortar joints, they attained failure load about 15% lower than the specimens made of a single tuff block. It can be supposed that for these specimens the mortar joints could have negatively influenced the alignment of the grid and the perfect adherence of the grid to the support.

Figure 7a and 7b plot the axial strain versus the applied load and the distribution of the axial strain along the reinforcement, respectively, for the specimen SB\_BN\_1.

In Figure 7a also the theoretical lines corresponding to the experimental average stiffness of both the only grid and the composite system ( $E_1$  and  $E_2$ , see Table 3) are plotted. The graph shows that the strain gauge 1, the closest to the loaded end, has measured larger values of strain compared with the ones positioned more distant. After a linear behaviour, the measures of strain gauge 1 tend to that of the uncracked composite system (slope  $E_1$ ), but they do not never attain the theoretical values of the grid or of the cracked composite system (slope  $E_2$ ), meaning that the strains in the grid are far from their tensile failure values. This can be observed also considering the maximum values of the first strain gauge listed in Table 5,  $\varepsilon_{max,exp}$ , since they were very lower than the theoretical values of the dry rovings in the unbonded area (i.e.  $\varepsilon_{max}$ ). Figure 7a shows that after the linear branch, for load levels higher than about 3 kN, the behaviour of strain gauge 1 becomes non-linear. Such a behaviour is due to the beginning of a debonding process in the first 70 mm;

after 3 kN, the strains, indeed, start increasing relevantly and tend to the theoretical values of the uncracked composite system (slope  $E_1$ ), supposed unbonded. When the first part of the composite starts debonding, it is not able to transfer anymore shear stresses to the masonry support, and, thus, is simply loaded in tension and cracking phenomena could occur in the grout. This justifies that the strains measured by the strain gauge 1 at about 3.4-3.5 kN overcome the theoretical values corresponding to  $E_1$ . If the grout was completely cracked, the behaviour of strain gauge 1 should tend to that of the only grid or of the cracked composite system (slope  $E_2$ ), but this does not verify, since the tension failure of the dry fibers occurred before. More information about the cracking pattern developed in the grout could be achieved by using the technique of Digital Image Correlation.

On the contrary, the behaviour of strain gauges 2 and 3 remains linear until failure of the specimen since they are positioned in a zone where the bond transfer was already expired.

The results highlighted by Figure 7a are confirmed by Figure 7b, where the strain at  $x=0$  has been evaluated theoretically by dividing the experimental applied force to the axial stiffness of the uncracked composite system ( $E_1 \cdot A$ , being  $A$  the area of composite). The strain distribution along the grid confirms that after 3 kN a debonding process start developing in the first 70 mm. Moreover, the distribution of axial strain shows that the bond transfer from the reinforcement to the tuff was effective and exhausted in the first 70 mm (i.e. the position of the first strain gauge), since the strains measured in the remaining part were very low. The propagation of debonding along the reinforcement was not observed and, thus, the strains remain very low, since the failure in tension of the dry fibers occurred before.

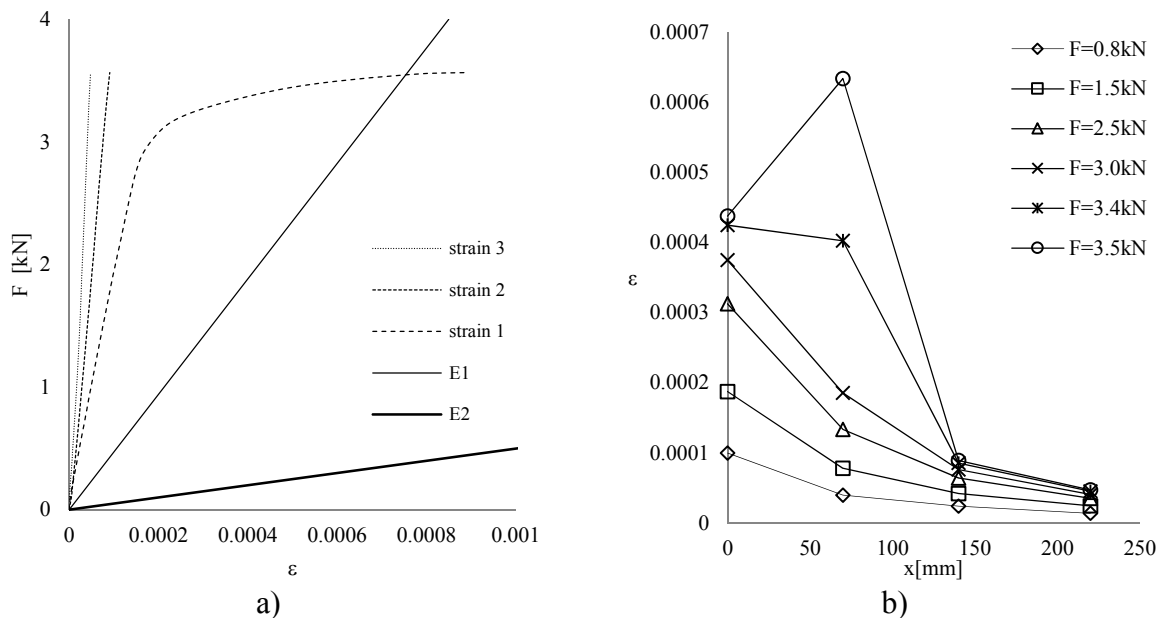


Figure 7: Specimen SB\_BN\_1: a) Experimental axial strain vs. Load; b) Distribution of axial strain along the reinforcement.

It is worth to note that the strain gauge measure the strain of a single longitudinal roving that could be reduced by two effects: a) the relevant contribution of the cementitious mortar that is also reinforced by short glass fibers spread in the matrix; and b) the interlocking contribute of the transversal rovings. Both phenomena could have an influence into determining a transfer bond length of about 70 mm, as experimentally observed for such a type of FRG system. It is worth to note that the Digital Image Correlation technique could be useful also for better investigating these aspects.

## **4 Conclusions and future research**

A series of 12 shear bond tests were performed according to a single push-pull set-up on tuff elements externally strengthened with FRG composites aimed to study the bond behaviour. The FRG composite investigated in this study is comprised of a glass fibre net and a non-cementitious matrix added of short glass fibers. The reinforcement was applied on both single tuff blocks and prisms made of three tuff blocks connected by two mortar joints. For each material (grout, mortar, tuff, composite), the mechanical properties were obtained through specific experimental tests.

Local pull-off tests were also performed to preventively check the quality of the bond between the grout and the tuff. A good bond behaviour was confirmed by both pull-off tests and bond tests evidencing that, therefore, the use of inorganic matrix instead of epoxy polymers for strengthening masonry structures is suitable.

An initial debonding was observed in some specimens in the first 50-70 mm of the bonded length, but in all tests the tensile failure of the dry grid in the unbonded area occurred before a real and complete debonding could develop. This results is due to the fact that the reinforcement percentage of the tested FRG system is lower than the values usually adopted for epoxy bonded FRP systems. The bond strength of the FRG-tuff interface could be, thus, comparable with the strength related to the tensile properties of the grid. Measures of strain gauges indicated a bond transfer length of about 70 mm.

Contrary to what was observed in previous experiments conducted with epoxy matrix on the same support, the presence of mortar joints has given a negative influence on the experimental result and, in particular, reduced the failure load of about 15%. Both tensile and bond tests evidenced that the grout gives a relevant contribute in carrying the load, especially before cracking, and that also after cracking a significant tension stiffening effect occurs, mainly due to the presence of short glass fibers in the grout mix.

The experimental results show the possibility and the opportunity to extent the experimental program: new tests are in progress aimed to highlight the influence of the geometrical and mechanical properties of the composite material on the bond of strengthening system. In particular, higher fiber percentage will be used, even if such strengthening system is generally applied over the entire surface of the

masonry wall, and therefore requires less transfer forces per unit area compared to systems with epoxy bonded FRP strips.

Due to the uncertainty in interpreting the local measures of strain gauges and aimed to have more information about the cracking pattern in the grout, in the next experimental tests the technique of Digital Image Correlation will be used for the evaluation of the strains in the reinforcement system.

## References

- [1] Mazzotti, C. and Murgu, F. (2015). "Numerical and experimental study of GFRP-masonry interface behavior: Bond evolution and role of the mortar layers." *Composites Part B: Engineering*, 10.1016/j.compositesb.2015.01.034, 212-225.
- [2] Hosseini, A., Mostofinejad, D., and Emami, M. (2015). "Influence of bonding technique on bond behavior of CFRP-to-clay brick masonry joints: Experimental study using particle image velocimetry (PIV)." *International Journal of Adhesion and Adhesives*, 10.1016/j.ijadhadh.2015.01.015, 27-39.
- [3] Ghiassi, B., Xavier, J., Oliveira, D., Kwiecien, A., Lourenço, P., and Zajac, B. (2015). "Evaluation of the bond performance in FRP-brick components re-bonded after initial delamination." *Composite Structures*, 10.1016/j.compstruct.2014.12.047, 271-281.
- [4] Garofano A., Ceroni F., Pecce M. (2014). Effect of the Presence of Mortar Joints in the Bond Behaviour of Tuff Masonry Elements, *Proc. of Murico4*, 9-11 September, 2014, Ravenna, Italy, ISBN-13:978-3-03835-203-7, Key Engineering Materials, Vol. 624, pp. 526-533.
- [5] Carozzi F.G. and Poggi, C. (2014). Mechanical properties and debonding strength of Fabric Reinforced Cementitious Matrix (FRCM) systems for masonry strengthening, *Composite Structures*, Elsevier, 107, 711-725.
- [6] De Santis S. and de Felice G. (2015). Tensile behaviour of mortar-based composites for externally bonded reinforcement systems. *Composites: Part B* 68 (2015) 401–413.
- [7] Badanoiu A. and Holmgren J. (2003). Cementitious composites reinforced with continuous carbon fibres for strengthening of concrete structures. *Cement & Concrete Composites* 25 (2003) 387–394.
- [8] D'Ambrisi A., Feo L., Focacci F. (2013). Experimental and analytical investigation on bond between Carbon-FRCM materials and masonry. *Composites: Part B* 46 (2013) 15–20.
- [9] Ombres L. (2015). Analysis of the bond between Fabric Reinforced Cementitious Mortar (FRCM) strengthening systems and concrete, *Composite Part B*, Elsevier, 69, 418-426.
- [10] D'Ambrisi A., Feo L., Focacci F. (2012). Bond-slip relations for PBO-FRCM materials externally bonded to concrete. *Composites: Part B* 43 (2012) 2938–2949.

- [11] D'Antino T., Carloni C., Sneed L.H., Pellegrino C. (2014). Matrix–fiber bond behavior in PBO FRCM composites: A fracture mechanics approach. *Engineering Fracture Mechanics* 117 (2014) 94–111.
- [12] Garofano A., Ceroni F., Pecce M. (2014). Effect of the Presence of Mortar Joints in the Bond Behaviour of Tuff Masonry Elements, *Proc. of Murico4*, 9-11 September, 2014, Ravenna, Italy, ISBN-13:978-3-03835-203-7, *Key Engineering Materials*, Vol. 624, pp. 526-533.
- [13] Faella C., Martinelli E., Nigro E., Paciello S. (2010). Shear capacity of masonry walls externally strengthened by a cement-based composite material: An experimental campaign. *Construction and Building Materials* 24 84–93.
- [14] Ceroni F., Garofano A., Pecce M. (2014). FE modelling of masonry panels externally bonded with FRP grid, *Proc. of 2<sup>nd</sup> International Conference on Protection of Historical Constructions, Prohitech*, 7-9 May 2014, Anthalya, Turkey, pp. 161-167, Boaziçi University Publishing; F. M. Mazzolani, G. Altay (Eds), ISBN 978-975-518-361-9.